9 Polarization and Depolarization of Light

M.I. Mishchenko and L.D. Travis

NASA Goddard Institute for Space Studies,
2880 Brodway, New York, New York 10025, U.S.A.

Abstract. Electromagnetic scattering by a small particle or a collection of small particles can produce light with polarization characteristics different from those of the incident beam. If the incident beam is unpolarized, the scattered light generally has at least one nonzero Stokes parameter other than intensity, and this phenomenon is often called "polarization." When the incident beam if fully linearly or circularly polarized, the scattered light may become partially polarized or even totally unpolarized, and this phenomenon is called "depolarization." In this paper we use exact solutions of Maxwell's equations and the vector radiative transfer equation to study the dependence of polarization and depolarization on such characteristics of scattering particles as size, refractive index, and shape. We also discuss the use of polarization and depolarization phenomena in remote sensing studies and particle characterization.

1 Introduction

The polarization state of a beam of light is traditionally described by a vector $\mathbf{I} = (I, Q, U, V)^T$ composed of four Stokes parameters (T means transpose). The first Stokes parameter, $\mathbf{I}$, is the intensity, while the other three parameters describe the polarization state of the beam. The Stokes parameters are always defined with respect to a reference plane, e.g., with respect to the meridional plane of the beam in a spherical coordinate system (Fig. 1):

$$I = E_\vartheta E_\vartheta^* + E_\varphi E_\varphi^*, \tag{1}$$

$$Q = E_\vartheta E_\vartheta^* - E_\varphi E_\varphi^*, \tag{2}$$

$$U = -E_\vartheta E_\varphi^* - E_\varphi E_\vartheta^*, \tag{3}$$

$$V = i(E_\varphi E_\vartheta^* - E_\vartheta E_\varphi^*), \tag{4}$$

where E_ϑ and E_φ are electric field components and the asterisk denotes a complex conjugate value [1]. The scattering of a beam of light by a single

F. Moreno and F. González (Eds.): Lectures 1998, LNP 534, pp. 159−175, 2000.

particle or a collection of particles is fully characterized by a 4x4 matrix **F** (often called the Mueller matrix) which describes the transformation of the Stokes vector of the incident beam into the Stokes vector of the scattered beam.

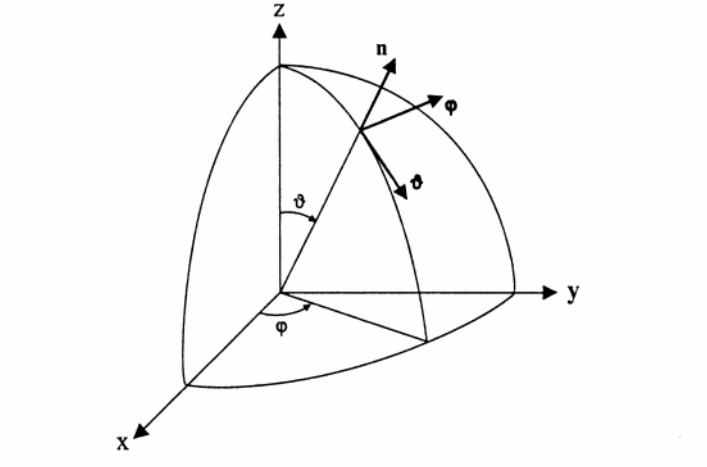

Fig. 1. Spherical coordinate system used to define the Stokes parametres of a beam of light propagating in the direction specified by the unit vector **n**.

$$\mathbf{I}^{sca} = \mathbf{F}\mathbf{I}^{inc}. \tag{5}$$

Electromagnetic scattering most typically produces light with polarization characteristics different from those of the incident beam. If the incident beam is unpolarized, the scattered light generally has at least one nonzero Stokes parameter other than intensity, and this phenomenon is often called "polarization." When the incident beam is fully linearly ($I = Q, U = V = 0$) or circularly ($I = V, Q = U = 0$) polarized, the scattered light may become partially polarized or even totally unpolarized, and this phenomenon is called "depolarization." Polarization and depolarization can be caused by both single and multiple scattering and depend on geometrical and physical characteristics of the scattering particle(s) such as shape, morphology, refractive index, size parameter (ratio of the particle circumference to the wavelength of the incident light), and orientation with respect to the coordinate system.

In this paper we analyze polarization and depolarization mechanisms for single scatterers and multi-particle configurations using exact numerical solutions of Maxwell's equations and the vector radiative transfer equation. We also discuss how the strong sensitivity of polarization and depolarization to

particle parameters makes both phenomena a powerful tool in remote sensing studies and particle characterization.

2 Single Scattering

Consider single scattering by a small-volume element composed of a collection of sparsely distributed, independently scattering particles (see the following section for a discussion of what interparticle separation makes the particles independent scatterers). For simplicity, we will assume that the incident beam is directed along the z axis and consider scattering in the xz plane. In this case the xz plane is also the scattering plane and the zenith angle of the scattered beam ϑ is also the scattering angle, Θ. If the particles comprising the small-volume element are randomly oriented and have a plane of symmetry, the Mueller matrix has the well-known, simplified block-diagonal structure, [2].

$$\mathbf{F}(\Theta) = \begin{bmatrix} F_{11} & F_{12} & 0 & 0 \\ F_{12} & F_{22} & 0 & 0 \\ 0 & 0 & F_{33} & F_{34} \\ 0 & 0 & -F_{34} & F_{44} \end{bmatrix}, \tag{6}$$

and has only six independent elements. It is easily seen from (5) and (6) that the Stokes vector of the scattered light is given by

$$\mathbf{I}^{sca} = \begin{bmatrix} F_{11}I^{inc} + F_{12}Q^{inc} \\ F_{12}I^{inc} + F_{22}Q^{inc} \\ F_{33}U^{inc} + F_{34}V^{inc} \\ -F_{34}U^{inc} + F_{44}V^{inc} \end{bmatrix} \tag{7}$$

and, in general, differs from $\mathbf{I}^{inc}$. Even if the incident beam is unpolarized, i.e., $\mathbf{I}^{inc} = (I, 0, 0, 0)^T$, the scattered beam has a nonzero Stokes parameter Q, unless the (1,2) element of the Mueller matrix is equal to zero. [The latter is always true in the exact forward ($\Theta = 0$) and exact backward ($\Theta = \pi$) directions.] This phenomenon is usually called polarization.

Figure 2 shows the phase function defined as

$$p(\Theta) = 2F_{11}(\Theta) / \int_0^\pi F_{11}(\Theta') \sin\Theta' d\Theta' \tag{8}$$

and the normalized Mueller matrix elements for a power law size distribution of spheres and surface-equivalent, randomly oriented oblate spheroids [3] with an aspect ratio of 1.7. The refractive index is 1.53+0.008i and the effective size parameter of the size distribution, χ_{eff}, is 15. The computations

were performed using the conventional Lorenz-Mie theory for spheres [2] and the T-matrix method for spheroids [3]. There are several obvious differences between the Mueller matrix elements for spheres and spheroids. The phase function for spheroids exhibits an enhanced side-scattering and a suppressed backscattering. The (1,1) and (2,2) elements for spheres are the same, whereas for spheroids they are significantly different. The same is true for the (3,3) and (4,4) elements. The degree of linear polarization $-F_{12}/F_{11}$ for spheroids is positive at side-scattering angles and is negative for spheres. We thus see that the elements of the Mueller matrix are highly sensitive to particle shape. Figures 3 and 4 as well as extensive computations reported by Hansen and

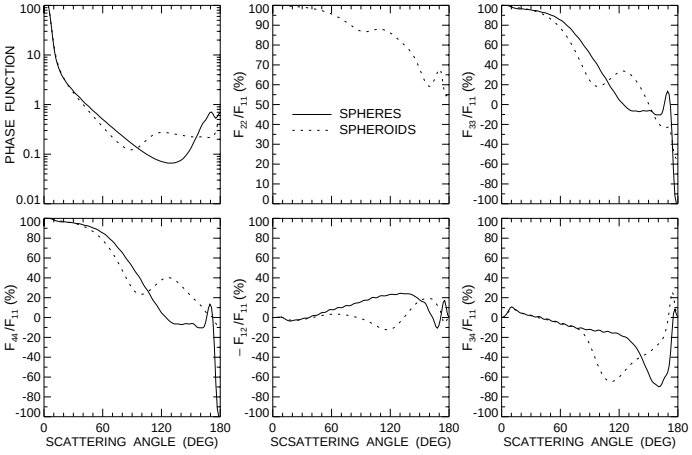

Fig. 2. Phase function and normalized Mueller matrix elements for a power law size distribution of spheres and randomly oriented spheroids. The refractive index is 1.53+0.008i and the effective size parameter of the size distribution is 15.

Travis [4], Mishchenko and Travis [5], Mishchenko et al. [3], and Mishchenko and Travis [6] show that they are equally sensitive to the particle refractive index and size parameter. This sensitivity makes accurate measurements of the Mueller matrix a valuable means of particle characterization.

In the exact backscattering direction, the Mueller matrix becomes diagonal and has only two independent elements [7]:

$$\mathbf{F}(\pi) = diag[F_{11}(\pi), F_{22}(\pi), -F_{22}(\pi), F_{11}(\pi) - 2F_{22}(\pi)]. \tag{9}$$

Assume now that the incident beam is 100% linearly polarized parallel to the scattering plane so that $\mathbf{I}^{inc} = I^{inc}(1,1,0,0)^T$. The second Stokes parameter of the backscattered signal is not, in general, equal to the first Stokes parameter and this phenomenon is traditionally called linear depolarization. The linear depolarization ratio, i.e., the ratio of the flux of the

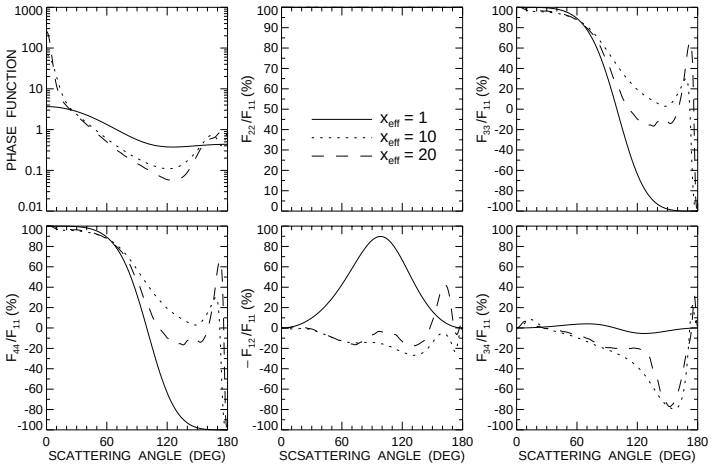

Fig. 3. Phase function and normalized Mueller matrix elements for a narrow gamma size distribution of spheres. The refractive index is 1.45 and the effective size parameter of the size distribution varies from 1 to 20.

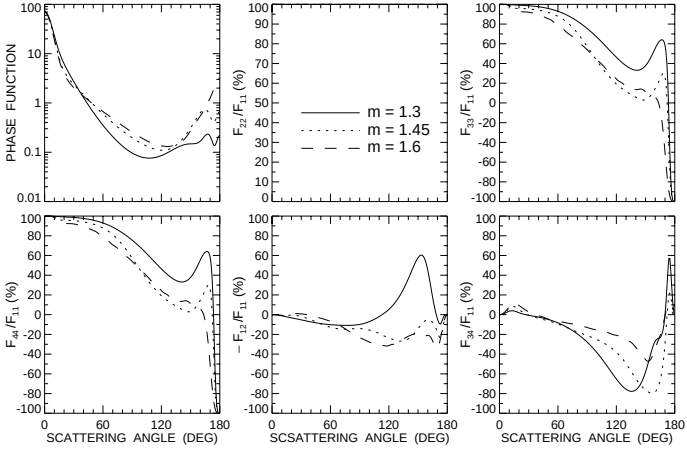

Fig. 4. As in Fig. 3, but for a fixed effective size parameter of 10 and refractive index m varying from 1.3 to 1.6.

cross-polarized component of the backscattered light relative to that of the co-polarized component, can be written as [see (9)]

$$\delta_L = \frac{I^{sca} - Q^{sca}}{I^{sca} + Q^{sca}} = \frac{F_{11}(\pi) - F_{22}(\pi)}{F_{11}(\pi) + F_{22}(\pi)}. \tag{10}$$

Similarly, we can consider a fully circularly polarized incident beam with Stokes parameters $I^{inc}(1, 0, 0, 1)^T$ to define the circular depolarization ratio

$$\delta_C = \frac{I^{sca} + V^{sca}}{I^{sca} - V^{sca}} = \frac{F_{11}(\pi) + F_{44}(\pi)}{F_{11}(\pi) - F_{44}(\pi)} = \frac{F_{11}(\pi) - F_{22}(\pi)}{F_{22}(\pi)}. \qquad (11)$$

It is straightforward to show that there is a direct relationship between the linear and circular depolarization ratios [cf. (10) and (11)]:

$$\delta_C = 2\delta_L/(1 - \delta_L). \qquad (12)$$

Spherically symmetric particles produce zero depolarization since in this case $F_{11}(\pi) = F_{22}(\pi)$ [2]. For particles without spherical symmetry, the latter equality does not generally hold and such particles can depolarize backscattered light. This explains why the linear and circular depolarization ratios can be direct indicators of particle nonsphericity. It is readily verified [7] that δ_L never exceeds 1 and

$$0 \leq 2\delta_L \leq \delta_C \leq \infty. \qquad (13)$$

Figure 5 shows the results of T-matrix computations of the linear depolarization ratio for a power law size distribution of randomly oriented nonspherical particles with a refractive index of 1.311 [8]. For spheroids, ϵ is the ratio of the largest to the smallest semi-axes. The shapes of prolate and oblate cylinders are specified by length-to-diameter and diameter-to-length ratios, respectively. The shape of second-order Chebyshev particles in a spherical coordinate system is described by the equation $R(\vartheta, \varphi) = R_0(1 + \epsilon cos 2\vartheta)$, where ϵ is a deformation parameter specifying the maximal deviation of the particle shape from that of a sphere with radius R_0 [9].

Figure 5 demonstrates that an interesting feature of the linear depolarization ratio for essentially all shapes considered is a rapid increase with increasing effective size parameter from 0 to about 5. Furthermore, maximal δ_L values for most shapes are observed at effective size parameters close to and sometimes smaller than 10. Since geometric optics concepts of rays, reflections, and refractions are inapplicable to wavelength and sub-wavelength sized particles, our computations suggest that multiple internal reflections in very large particles, as discussed by Liou and Lahore [10], are not the only mechanism of producing depolarization and not necessarily the mechanism producing maximal δ_L values. For example, the peak δ_L value for polydisperse prolate spheroids with $\epsilon = 1.2$ is close to 0.7 and is reached at χ_{eff} as small as 12.5. Also, geometric optics predicts size-parameter-independent depolarization ratios for nonabsorbing particles, whereas exact T-matrix computations for monodisperse scatterers show strong oscillations of δ_L with varying particle size [7]. It thus appears that resonance effects in small nonspherical particles can be an efficient alternative mechanism of producing strong depolarization.

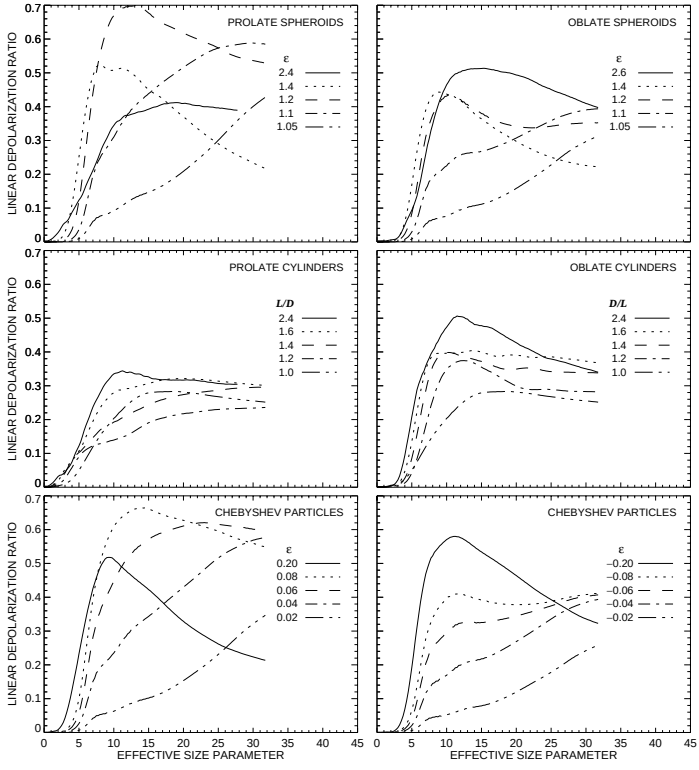

Fig. 5. Linear depolarization ratio versus effective size parameter for polydisperse, randomly oriented particles of different shapes. The refractive index is 1.311.

The computations also show that although nonzero depolarization values directly indicate the presence of nonspherical particles, there is no simple relationship between δ_L and the degree of particle asphericity (i.e., ratio of the largest to the smallest particle dimensions). Even spheroids with ϵ as small as 1.05 (2.5% deviation from the perfect spherical shape) and Chebyshev particles with $|\epsilon|$ as small as 0.02 already produce strong depolarization. The largest δ_L values are produced by prolate spheroids with aspect ratio as small as 1.2 and Chebyshev particles with ϵ as small as 0.08-0.10 (8-10% deviation from a sphere). Furthermore, δ_L for spheroids and, especially, cylinders seems to saturate with increasing aspect ratio. Also of interest is that smooth scatterers (spheroids and Chebyshev particles) produce depolarization ratios comparable to and even exceeding those for sharp-edged cylinders.

3 Multiple Scattering

Cooperative effects in multi-particle configurations can significantly modify the process of polarization and depolarization. In particular, it appears that polarization is an intrinsically single-scattering phenomenon which can be significantly attenuated by multiple scattering. On the other hand, cooperative effects cause nonzero depolarization values even for clusters consisting of spherical particles and often reinforce depolarization caused by particle nonsphericity.

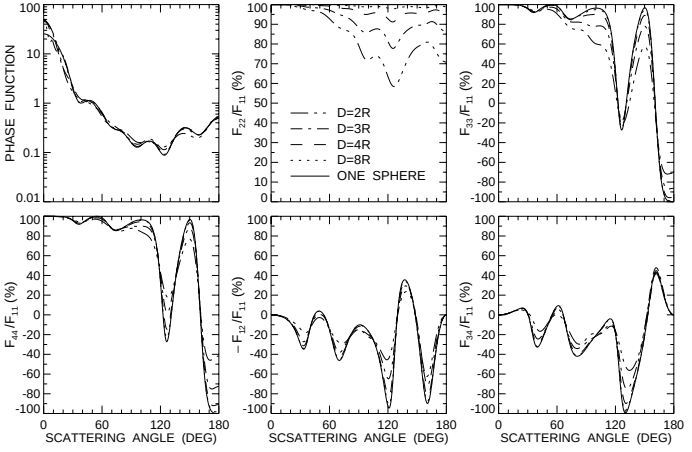

Fig. 6. Phase function and normalized elements of the Mueller matrix for randomly oriented bispheres with touching and separated components.

We will demonstrate this by considering the simplest configuration composed of two identical spheres with touching or separated components. Figure 6 shows the results of T-matrix computations of the phase function and the normalized elements of the Mueller matrix for randomly oriented bispheres with an index of refraction of 1.5 + 0.005i [11]. The size parameter of the component spheres is 5 and the distance D between the sphere centers varies from twice their radius for touching spheres to eight times their radius for "widely" separated spheres. For comparison, solid curves show the results of Lorenz-Mie computations for a single sphere with the same size parameter 5 and represent the case of a bisphere with infinitely separated components. The oscillations in the single-sphere curves are a manifestation of the interference structure typical of monodisperse spheres and are traditionally attributed to interference of light diffracted and refracted/reflected by the particle [4]. It is obvious that the magnitude of these oscillations decreases as the component spheres become closer and is minimal for the bisphere with touching components. Since the cooperative effects strengthen as the interparticle di-

stance decreases, Fig. 6 unequivocally demonstrates that the most obvious effect of cooperative effects in multi-particle configurations is to suppress the single-sphere signature in the elements of the Mueller matrix. In particular, the degree of linear polarization $-F_{12}/F_{11}$ becomes more neutral and less indicative of the physical characteristics of the component spheres.

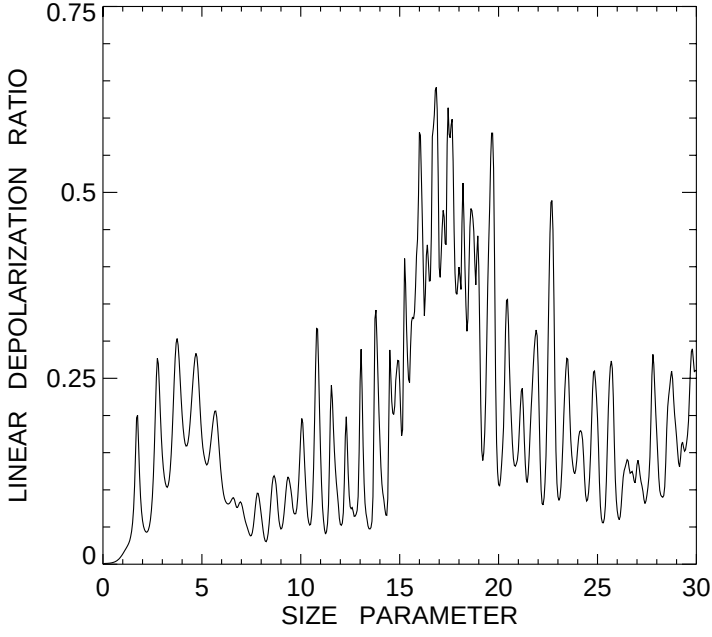

Fig. 7. Linear depolarization ratio versus component-sphere size parameter for randomly oriented bispheres with touching components. The refractive index is 1.5 + 0.005i.

The only exception is the ratio F_{22}/F_{11}, which is identically equal to 1 for single spheres but increasingly deviates from 1 with decreasing distance between the bisphere components. As follows from (10), the deviation of this ratio from 1 results in increasingly nonzero values of the linear depolarization ratio. Therefore, we must conclude from (10) and Fig. 6 that although single spheres do not depolarize light, cooperative effects in multi-sphere aggregates can produce significant depolarization. Figure 7 shows δ_L as a function of size parameter for randomly oriented bispheres with touching components [12] and demonstrates rather large δ_L values even for the simplest multi-particle configuration.

It is interesting to note that as small a distance between the sphere centers as 4 times their radius makes the bisphere Mueller matrix elements very close to those of a single sphere (Fig. 6). This result provides an important

quantitative criterion of what minimal distance between wavelength-sized particles makes them independent scatterers [12].

Multiple scattering in optically thick discrete random media has similar effects on polarization and depolarization. For example, Hansen and Travis [4] use numerically exact adding/doubling computations of polarized radiative transfer in a plane-parallel atmosphere composed of spherical particles and show that the polarization signature becomes more neutral and featureless as the optical thickness of the cloud increases, i.e., when the amount of multiple scattering grows (Fig. 8). Similarly, they demonstrate that the polarization feature is most pronounced in the first-order-scattering contribution to the reflected light and diminishes as more orders of scattering are taken into account.

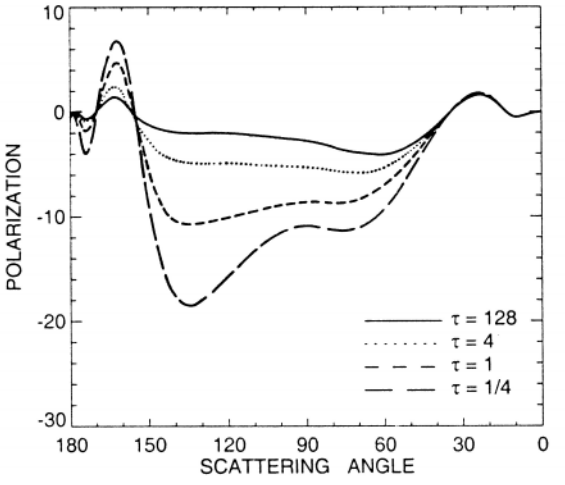

Fig. 8. Degree of linear polarization of reflected light, $-I/Q(\%)$, integrated over the disk of a locally-plane-parallel planet uniformly covered with a cloud layer of varying optical thickness τ and illuminated by an unpolarized beam of light. The cloud particles are modeled by a narrow gamma size distribution of spheres with an effective radius of 1 μm and refractive index 1.44. The wavelength of the incident light is 0.55 μm.

The computation of the depolarization ratios for optically thick discrete random media is a more complicated problem because the Stokes parameters of light reflected in the vicinity of the exact backscattering direction are affected by a phenomenon called coherent backscattering or weak photon localization (e.g., POAN Research Group [13]). This phenomenon is caused by constructive interference of light travelling along the same multiple-scattering paths but in opposite directions and is not explicitly described by the radiative transfer equation. However, Mishchenko [14] used the general reciprocity

principle to prove that the solution of the vector radiative transfer equation [15,16] can still be used to exactly calculate the coherent backscattering contribution in the strict backscattering direction. Specifically, the total Mueller matrix in the exact backscattering direction has the structure given by (6) and can be represented in the form

$$\mathbf{F} = \mathbf{F}^1 + \mathbf{F}^L + \mathbf{F}^C, \tag{14}$$

where $\mathbf{F}^1$ is the first-order-scattering contribution, $\mathbf{F}^L$ is the incoherent contribution of orders of scattering 2 and higher, and the matrix $\mathbf{F}^C$ represents the coherent contribution and is expressed in the matrix $\mathbf{F}^L$ as follows:

$$F_{ij}^C = F_{ij}^L, \qquad i \neq j, \tag{15}$$

$$F_{11}^C = \frac{1}{2}(F_{11}^L + F_{22}^L - F_{33}^L + F_{44}^L), \tag{16}$$

$$F_{22}^C = \frac{1}{2}(F_{11}^L + F_{22}^L + F_{33}^L - F_{44}^L), \tag{17}$$

$$F_{33}^C = \frac{1}{2}(-F_{11}^L + F_{22}^L + F_{33}^L + F_{44}^L), \tag{18}$$

$$F_{44}^C = \frac{1}{2}(F_{11}^L - F_{22}^L + F_{33}^L + F_{44}^L). \tag{19}$$

Since the matrices $\mathbf{F}^1$ and $\mathbf{F}^L$ can be found by solving numerically the vector radiative transfer equation, (14)-(19) render the total backscattering Mueller matrix. Note that the angular width of the coherent backscattering effect is negligibly small for dilute particle distributions such as clouds, but is significant for media composed of densely packed particles such as snow or sand layers.

As an example, Fig. 9 shows the linear depolarization ratio versus cosine of the angle of incidence μ_0 for a semi-infinite medium composed of spherical particles with an effective size parameter of 10 and refractive indices 1.2 and 1.6 [17]. It is seen that δ_L is zero in the limit $\mu_0 \to 0$, i.e., when only the light scattered once contributes to the total reflected signal. This first-order-scattering contribution is not depolarized because the particles forming the medium are assumed to be spherical. However, at normal incidence ($\mu_0 = 1$) the multiple-scattering contribution to the total backscattered signal

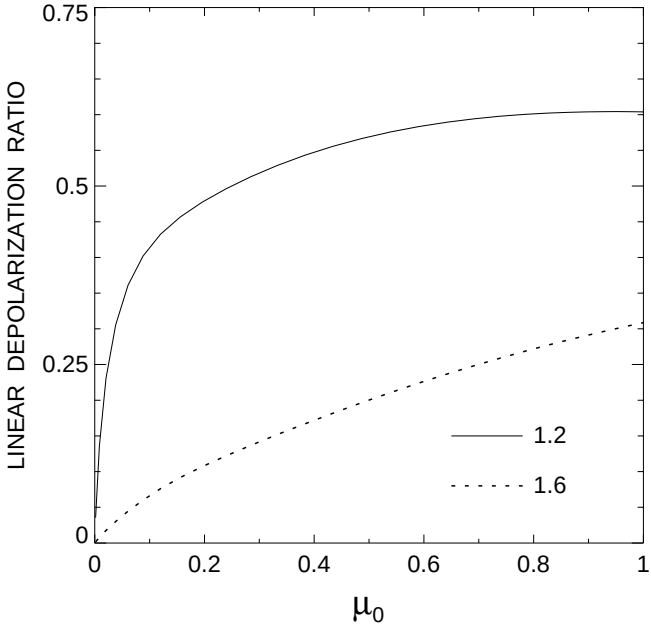

Fig. 9. Linear depolarization ratio versus cosine of the angle of incidence for backscattering by a semi-infinite homogeneous layer composed of polydisperse spherical particles with an effective size parameter of 10 and refractive indices 1.2 and 1.6.

is significant and results in strong depolarization. Figure 10 shows even larger values for the circular depolarization ratio. The numerical computations suggest that

$$\delta_L \leq 1 \qquad and \qquad \delta_L \leq \delta_C. \tag{20}$$

These properties of the depolarization ratios produced by multiple scattering are similar to those of the depolarization ratios caused by single scattering on nonspherical particles (cf. Sect. 2). This may make it difficult in many practical situations to distinguish between the two depolarization mechanisms.

4 Particle Characterization and Remote Sensing

Figure 11 exemplifies the use of Mueller matrix measurements for particle characterization and compares experimental data for a single latex sphere at a wavelength of 441.6 nm [2] and results of Lorenz-Mie computations. The refractive index of latex is well known (1.588), and it was also known from

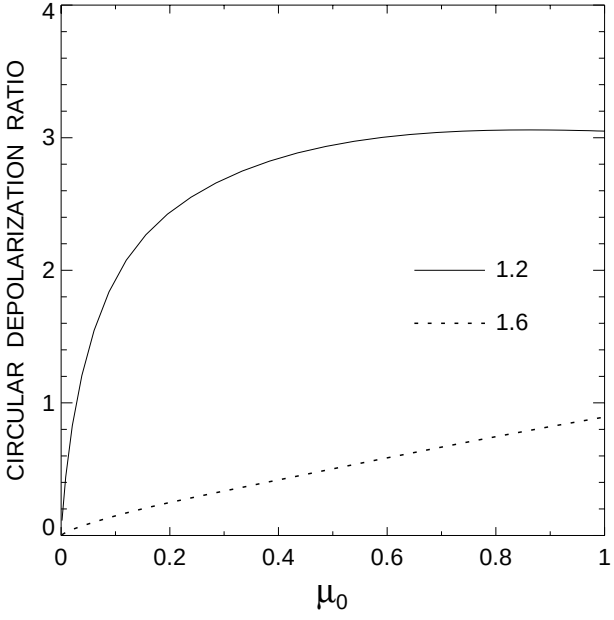

Fig. 10. As in Fig. 9, but for the circular depolarization ratio.

the manufacturer that the diameter of the latex particle was in the 1 μm range. The best-fit agreement between the measurements and computations was obtained for a diameter of 1122 nm, while computations for diameters 1108 and 1136 nm showed large discrepancies [11]. Figure 12 shows a similar example but for a single two-sphere cluster in random orientation. In this case the best fit was obtained for a component-sphere diameter of 1129 nm and the estimated accuracy of the retrieval was better than 20 nm [11]. These examples demonstrate the potential accuracy of particle sizing based on polarimetric measurements (see also Hirleman and Bohren [18]).

The strong sensitivity of polarization and depolarization on the physical characteristics of scattering particles has been widely employed in remote sensing studies. A classical example is the analysis of ground-based polarimetric observations of Venus which enabled Hansen and Hovenier [19] to determine the size and chemical composition of Venus cloud particles. This work was continued by Kawabata et al. [20], Sato et al. [21] and Knibbe et al. [22], who analyzed polarimetric observations provided by the Pioneer Venus orbiter. Mishchenko [6] used computations similar to those shown in Figs. 9 and 10 to explain the unusually large depolarization ratios measured at centimeter and decimeter wavelengths for the icy Galilean satellites of Jupiter [23]. Mishchenko [24] and Rosenbush et al. [25] have interpreted telescopic polarization observations of Saturn's rings and icy outer planet satellites in

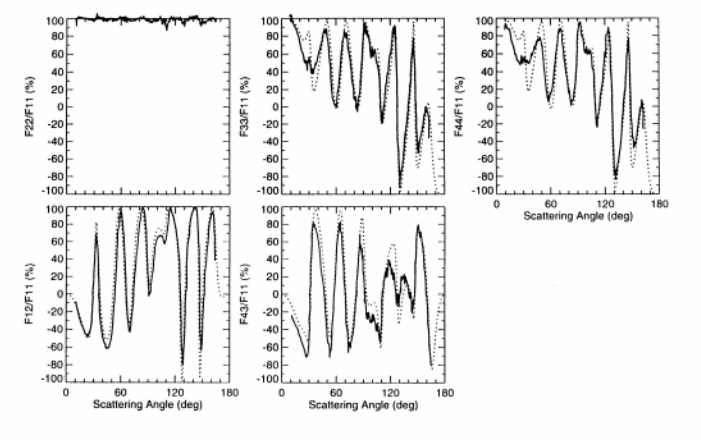

Fig. 11. Normalized Mueller matrix elements for a single latex sphere. Solid curves show measurements by Bottiger et al. [2] and the dotted curves show results of Lorenz-Mie computations.

terms of the polarization opposition effect produced by coherent backscattering and estimated the size of ice grains covering the surfaces of these solar system objects. Mishchenko and Sassen [8] used the computations shown in Fig. 5 to explain the frequent occurrence of large δ_L values for very young aircraft condensation trails (contrails) and concluded that observed increases of δ_L with the contrail's age can be explained either by a rapid increase of the particle size parameter from less than 1 to about 5 or by assuming that the contrail particles originate as perfect spheres and then acquire a certain degree of asphericity. Sassen [26] and Aydin [27] review the use of lidar and radar backscattering depolarization measurements for characterizing aerosol and cloud particles and precipitation. Liou et al. [28] discuss the potential of polarimetry in remote sensing of cirrus clouds, while Quinby-Hunt et al. [29], Lumme [30], and Hoekstra and Sloot [31] describe multiple applications of polarimetry in remote sensing of the marine environment and in characterizing interplanetary dust grains and biological microorganisms.

5 Acknowledgments

We thank Nadia Zakharova for help with graphics. This research was supported by the NASA EOS Program, NASA FIRE III Program, and NASA GACP Program.

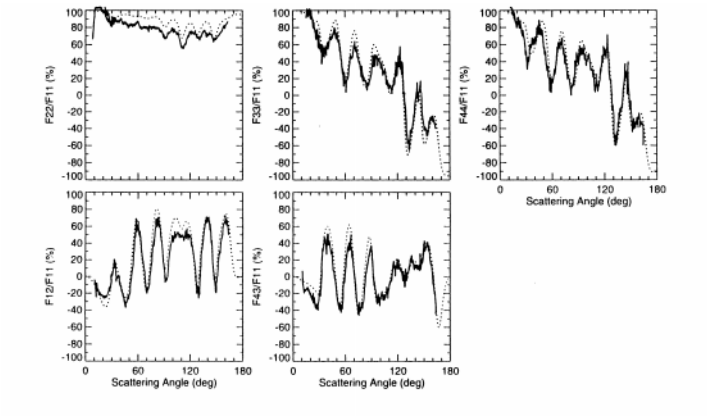

Fig. 12. Normalized Mueller matrix elements for a single latex bisphere in random orientation. Solid curves show measurements by Bottiger et al. [2] and the dotted curves show results of T-matrix computations.

References

1. Mishchenko M. I., Hovenier J. W. and Travis L. D. (1999): Concepts, Terms, Notation. Light Scattering by Nonspherical Particles: Theory, Measurements, and Applications, eds. M. I. Mishchenko, J. W. Hovenier and L. D. Travis (Academic Press, San Diego).
2. Bottiger J. R., Fry E. S. and Thompson R. C. (1980): Phase Matrix Measurements for Electromagnetic Scattering by Sphere Aggregates. Light Scattering by Irregularly Shaped Particles, ed. D. W. Schuerman (Plenum Press, New York), 283-290.
3. Mishchenko M. I., Travis L. D. and Mackowski D. W. (1996): T-Matrix Computations of Light Scattering by Nonspherical Particles: A Review. J. Quant. Spectrosc. Radiat. Transfer **55**, 535-575.
4. Hansen J. E. and Travis L. D. (1974): Light Scattering in Planetary Atmospheres. Space Sci. Rev. **16**, 527-610.
5. Mishchenko M. I. and Travis L. D. (1994): Light Scattering by Polydisperse, Rotationally Symmetric Nonspherical Particles: Linear Polarization. J. Quant. Spectrosc. Radiat. Transfer **51**, 759-778.
6. Mishchenko M. I. and Travis L. D. (1997): Satellite Retrieval of Aerosol Properties Over the Ocean Using Polarization as Well as Intensity of Reflected Sunlight. J. Geophys. Res.**102**, 16,989-17,013.
7. Mishchenko M. I. and Hovenier J. W. (1995): Depolarization of Light Backscattered by Randomly Oriented Nonspherical Particles. Opt. Lett. **20**, 1356-1358.
8. Mishchenko M. I. and Sassen K. (1998): Depolarization of Lidar Returns by Small Ice Crystals: An Application to Contrails. Geophys. Res. Lett. **25**, 309-312.
9. Wiscombe W. J. and Mugnai A. (1986): Single Scattering from Nonspherical Chebyshev Particles: A Compendium of Calculations. NASA Ref. Publ. 1157, NASA GSFC, Greenbelt, MD.

10. Liou K.-N. and Lahore H. (1974): Laser Sensing of Cloud Composition: A Backscattered Depolarization Technique. J. Appl. Meteorol. **13**, 257-263.
11. Mishchenko M. I. and Mackowski D. W. (1996): Electromagnetic Scattering by Randomly Oriented Bispheres: Comparison of Theory and Experiment and Benchmark Calculations. J. Quant. Spectrosc. Radiat. Transfer **55**, 683-694.
12. Mishchenko M. I., Mackowski D. W. and Travis L. D. (1995): Scattering of Light by Bispheres with Touching and Separated Components. Appl. Opt. **34**, 4589-4599.
13. POAN Research Group, ed. (1998): New Aspects of Electromagnetic and Acoustic Wave Diffusion (Springer, Berlin).
14. Mishchenko M. I. (1992): Enhanced Backscattering of Polarized Light from Discrete Random Media: Calculations in Exactly the Backscattering Direction. J. Opt. Soc. Am. A **9**, 978-982.
15. Chandrasekhar S. (1950): Radiative Transfer (Oxford Univ. Press, London).
16. Hovenier J. W. and van der Mee C. V. M. (1983): Fundamental Relationships Relevant to the Transfer of Polarized Light in a Scattering Atmosphere. Astron. Astrophys. **128**, 1-16.
17. Mishchenko M. I. (1997): Diffuse and Coherent Backscattering by Discrete Random Media. J. Quant. Spectrosc. Radiat. Transfer **56**, 673-702.
18. Hirleman E. D. and Bohren C. F. (eds.) (1991). Special Feature on Optical Particle Sizing. Appl. Opt. **30**, 4685-4986.
19. Hansen J. E. and Hovenier J. W. (1974): Interpretation of the Polarization of Venus. J. Atmos. Sci. **27**, 265-281.
20. Kawabata K., Coffeen D. L., Hansen J. E., Lane W. A., Sato M. and Travis L. D. (1980): Cloud and Haze Properties from Pioneer Venus Polarimetry. J. Geophys. Res. **85**, 8129-8140.
21. Sato M., Travis L. D. and Kawabata K. (1996): Photopolarimetry Analysis of the Venus Atmosphere in Polar Regions. Icarus **124**, 569-585.
22. Knibbe W. J. J., de Haan J. F., Hovenier J. W. and Travis L. D. (1998): Analysis of Temporal Variations of the Polarization of Venus Observed by Pioneer Venus Orbiter. J. Geophys. Res. **103**, 8557-8574.
23. Ostro S. J. (1993): Planetary Radar Astronomy. Rev. Mod. Phys. **65**, 1235-1279.
24. Mishchenko M. I. (1993): On the Nature of the Polarization Opposition Effect Exhibited by Saturn's Rings. Astrophys. J. **411**, 351-361.
25. Rosenbush V. K., Avramchuk V. A., Rosenbush A. E. and Mishchenko M. I. (1997): Polarization Properties of the Galilean Satellites of Jupiter: Observations and Preliminary Analysis. Astrophys. J. **487**, 402-414.
26. Sassen K. (1999). Lidar Backscatter Depolarization Technique for Cloud and Aerosol Research. Light Scattering by Nonspherical Particles: Theory, Measurements, and Applications, eds. M. I. Mishchenko, J. W. Hovenier, and L. D. Travis (Academic Press, San Diego).
27. Aydin K. (1999): Centimeter and Millimeter Wave Scattering From Nonspherical Hydrometeors. Light Scattering by Nonspherical Particles: Theory, Measurements, and Applications, eds. M. I. Mishchenko, J. W. Hovenier and L. D. Travis (Academic Press, San Diego).

28. Liou K. N., Takano, Y. and Yang P. (1999). Light Scattering and Radiative Transfer in Ice Crystal Clouds: Applications to Climate Research. Light Scattering by Nonspherical Particles: Theory, Measurements, and Applications, eds. M. I. Mishchenko, J. W. Hovenier, and L. D. Travis (Academic Press, San Diego).
29. Quinby-Hunt M. S., Hull P. G. and Hunt A. J. (1999): Polarized Light Scattering in the Marine Environment. Light Scattering by Nonspherical Particles: Theory, Measurements, and Applications, eds. M. I. Mishchenko, J. W. Hovenier and L. D. Travis (Academic Press, San Diego).
30. Lumme K. (1999): Scattering Properties of Interplanetary Dust Particles. Light Scattering by Nonspherical Particles: Theory, Measurements, and Applications, eds. M. I. Mishchenko, J. W. Hovenier and L. D. Travis (Academic Press, San Diego).
31. Hoekstra A. G. and Sloot P. M. A. (1999). Biomedical and Biophysical Applications of Non-Spherical Scattering. Light Scattering by Nonspherical Particles: Theory, Measurements, and Applications, eds. M. I. Mishchenko, J. W. Hovenier and L. D. Travis (Academic Press, San Diego).